The differential atomic response of the topmost graphene layer on graphite

2009 J. Phys.: Condens. Matter 21 195402

(http://iopscience.iop.org/0953-8984/21/19/195402)

J. Phys.: Condens. Matter **21** (2009) 195402 (8pp) doi:10.1088/0953-8984/21/19/195402

The differential atomic response of the topmost graphene layer on graphite

G S Khara[1] **and Jaewu Choi**[2,3]

[1] Department of Electrical and Computer Engineering, Wayne State University, 5050 Anthony Wayne Drive #3100, Detroit, MI 48202, USA
[2] Department of Information Display, Kyung Hee University, 1 Hoeki-Dong Dondaemoon-Ku, Seoul 130-701, Korea

E-mail: JaewuChoi@khu.ac.kr

Received 2 February 2009, in final form 3 March 2009
Published 7 April 2009
Online at stacks.iop.org/JPhysCM/21/195402

Abstract
The atomic response of the topmost graphene layer on graphite was studied by using scanning tunneling microscopy (STM) as a function of tunneling gap distance, gap voltage and bias polarity. The contrast of the site-dependent topographical image depends on the gap distance, and the site-dependent tunneling current order of magnitude at a given gap distance is switched with the gap voltage (i.e. the contrast is significantly altered). The site-dependent current order is altered at the lower positive gap voltage as the gap distance is reduced between the probe and the carbon atoms of the topmost graphene layer. The switching in the atomic image contrast and the current order of magnitude is directly related to the differential atomic response of carbon atoms to the STM probe originating from the electronically active and mechanically soft β-carbon atoms.

(Some figures in this article are in colour only in the electronic version)

1. Introduction

Allotropes of graphite, such as fullerene, carbon nanotubes and graphene, have become popular research materials because of their possible applications and unique physical properties related to their size and dimensionality [1–4]. Graphite is often a standard reference to understand the basic properties of these carbon allotropes. Among various types of graphite, highly oriented pyrolytic graphite (HOPG) has been primarily studied because of its highly crystalline properties.

HOPG has a Bernal structure, which is an ABAB physical stack of graphene layers, consisting of a sp^2 hybridization network. In this stacking order, there are two distinct types of carbon atoms, which have differences in their chemical environments. An α-carbon atom of a layer is located between two carbon atoms of the nearest graphene layers along the stacking direction (0001) while a β-carbon atom in a graphene layer is placed between two hollow (H) sites of the nearest graphene layers. The Bernal structure directly indicates that the α-carbon is mechanically stronger than the β-carbon along the stacking direction [5, 6].

[3] Author to whom any correspondence should be addressed.

The electronic interaction strength between α-atoms along the stacking direction is also stronger than that between β-atoms because the distance between the nearest α-atoms is half of the distance between the nearest β-atoms. Due to this difference in the strength of the interaction, the electronic structure within ± 0.8 eV near the Fermi level is largely determined by β-carbons rather than α-carbons and is symmetric with respect to the Fermi level [6, 7]. Therefore the electronic states of β-site carbons are active for tunneling at low gap voltages while the electronic states of α-site carbons are inactive [6–8]. The structure of HOPG clearly indicates that there are two types of surface carbon atoms with distinct electronic and mechanical properties.

The surface atomic and electronic structure of HOPG has been heavily studied by scanning tunneling microscopy (STM) and companion theoretical efforts [8–17]. The observed atomic structure of the graphite surface often shows a trigonal lattice with a spacing of 2.46 Å, over a wide range of STM imaging parameters. These imaged surface structures are different from the intrinsic hexagonal atomic lattice structure of the topmost graphene layer on graphite. Although rare, a hexagonal lattice structure with spacing of 1.42 Å has also been observed [10–12]. This latter atomic image

by STM is inconsistent with the known surface structure and therefore has been interpreted by various proposed imaging mechanisms [5, 9–18]. The generally accepted imaging mechanism is based on the site-dependent electronic band structure (electron density of the wavefunction and its symmetry) and mechanical strength (lattice rigidity), as explained above [5, 8].

In this study, we have investigated the site-dependent atomic response of the topmost graphene layer on graphite to a STM probe by varying the tunneling gap distance, gap voltage and voltage polarity. This study reveals that the site-dependent atomic response to the probe varies with the tunneling gap distance, gap voltage and voltage polarity. The site-dependent atomic image contrast is switched with the gap distance. The relative order of the site-dependent tunneling current is switched with a gap voltage higher than a critical voltage. The critical voltage depends on the gap distance and the polarity of the bias voltage. We suggest that the image contrast switching due to the probe–sample distance change and concomitant changes to the relative order of the site-dependent current in the voltage scans are due to the differential atomic response (motion) of carbon atoms to the STM probe. We suggest that, to a large extent, this local field-induced movement of surface carbon atoms, in response to the close proximity of a suitably biased STM tip, originates from the mechanically soft β-carbon atoms.

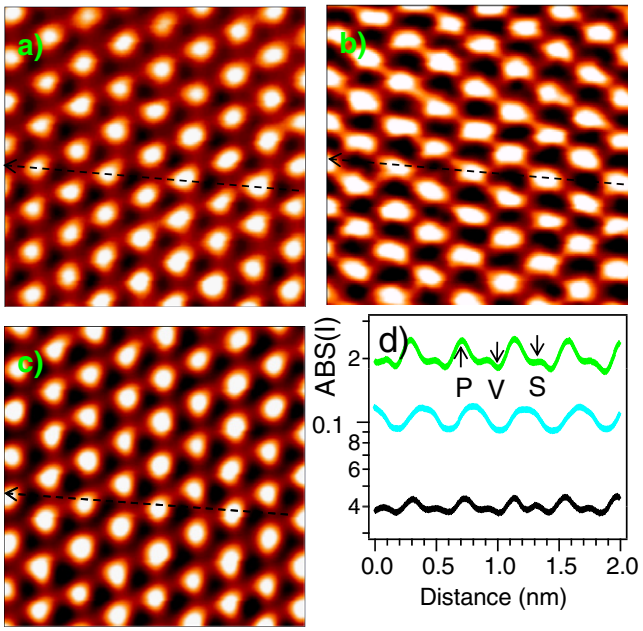

Figure 1. (Colour online) Topography images of HOPG were taken at set currents of (a) −40, (b) −100 and (c) −200 pA with −70 mV gap voltage. The size of images is 1.71 nm × 1.71 nm. (d) Line profiles of topographical images along the surface lattice (1, 1) are obtained as indicated by arrow lines. The peak, shoulder and valley in the line profile are indicated by P, S and V, respectively.

2. Experiment

A clean surface of HOPG was prepared in air by removing the top graphene layers using scotch tape [1]. The sample was investigated at $\sim 10^{-9}$ Torr at room temperature by using an Omicron UHV Micro SPM (scanning probe microscope). An electrochemically etched tungsten tip was employed for both the microscopic and spectroscopic studies. The topographical images were obtained with negative gap voltage of −70 mV applied to the sample at several feedback set currents from −40 to −200 pA with 1% loop gain. The scan speed was 30 nm s^{-1}.

For the site-dependent scanning tunneling spectroscopic (STS) study, the voltage was swept from −1.0 to 1.0 V at each spectroscopy location while the feedback is off. Tunneling current–voltage (I–V) spectra were obtained at three probe–sample distances (tunneling gap distance), d_1, d_2 and d_3 ($d_1 > d_2 > d_3$), which are controlled by the initial set current at −50 pA, −100 pA and −200 pA, respectively, while the gap voltage was maintained at a constant negative voltage of −70 mV. The 20 or 25 site-dependent STS datasets are taken and averaged.

3. The differential atomic response of the graphite surface

Figure 1 shows topographical images of the topmost graphene layer on HOPG taken at three gap distances, d_1, d_2 and d_3 ($d_1 > d_2 > d_3$). Topographical images taken at large and small tunneling gap distances d_1 (−40 pA) and d_3 (−200 pA) show the typical trigonal lattice structures with the barely visible underlying structures, as shown in figures 1(a) and (c). However, the topographical image taken at the intermediate gap distance d_2 (−100 pA) shows a distorted hexagonal-like structure with bright bar-like structures, as shown in figure 1(b). These are very different apparent structures while the bar-like structure shown in figure 1(b) has not been reported previously to the authors' knowledge.

The bar-like structure, as will be discussed later, has much to do with tip interactions and should be attributed to the repulsive interactions of the probe tip atom with the on-site carbon atom and to the attractive interactions of the probe tip atom with the nearest off-site carbon atoms. This results in the modification of the site-dependent current order of magnitude and image. In the discussion that follows, we present the arguments in support of this analysis.

Figure 1(d) shows line profiles of topographical images of figures 1(a)–(c) along the surface lattice (1, 1). The line profiles of figures 1(a) and (c) show three distinct peaks corresponding to the highest, the middle and the lowest spots, respectively. These are referred to as P (peak), S (shoulder) and V (valley), respectively, whereas the line profile taken from figure 1(b) only shows peak (P) and valley (V), as expected. The structure shown in figures 1(a) and (c) has been understood as imaging only specific carbon atoms, β-carbons [8–17]. The shape of the line profile, given the best understanding of the surface, is troublesome. The question arises why there are three distinct points as P, S and V instead of two, i.e. just peaks and valleys as shown in the line profile of figure 1(d). This is an additional complication to consider, in addition to the structure shown in figure 1(b).

We find that two distinct topographical points P and V, or three distinct points P, S and V, can be obtained by

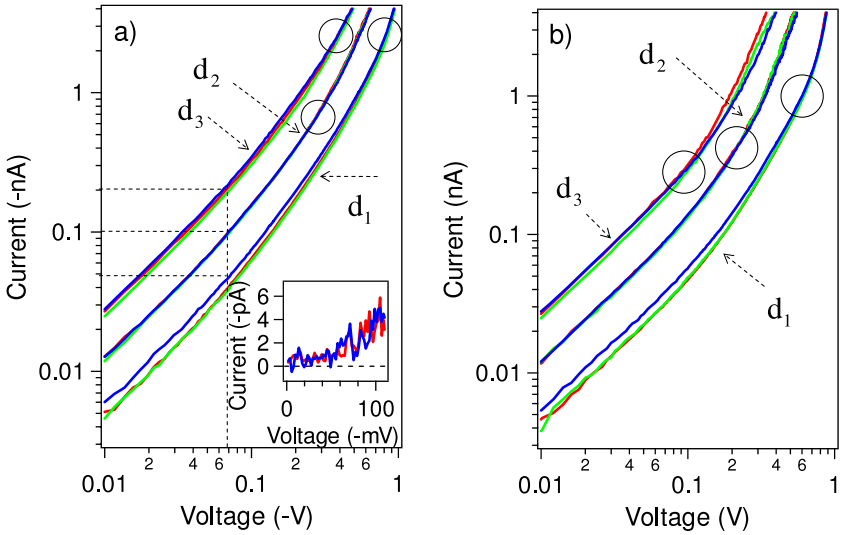

Figure 2. (Colour online) Site-dependent (peak: blue, shoulder: red and valley: green) tunneling I–V spectra are plotted in log–log scale at set currents of $-50(d_1)$, $-100(d_2)$ and -200 pA (d_3) for (a) negative gap voltage range of -1.0–0 V and (b) positive gap voltage range of 0–1.0 V. The inset of figure 2(a) is the difference current spectra of the peak and shoulder current spectra obtained at d_2. These are obtained by subtracting the current at the valley from the current spectra at the peak (blue) and shoulder (red), respectively.

controlling the STM probe to sample distance and the gap voltage. Figure 2 shows the site-dependent I–V curves taken at P (blue), S (red), and V (green) sites of the topographical images shown in figure 1, plotted in log–log scale at three different probe–sample distances, d_1, d_2 and d_3. Figure 2(a) shows the site-dependent tunneling I–V spectra for the negative gap voltage (the sample biased with negative gap voltage with respect to the STM probe) from -1 to 0 V while figure 2(b) does the same for the positive gap voltage from 0 to $+1$ V.

When negative bias voltage is applied to the sample, the site-dependent I–V curves are distinguishable at the gap distances of d_1 and d_3 but they becomes indistinguishable when the gap voltage is higher in magnitude than 0.8 V and 0.5 V at d_1 and d_3, respectively. This suggests that the electrostatic interaction plays the role in the site-dependent I–V curves.

The STM probe tip to sample spacing of d_2 is actually different than the larger and smaller spacing for more than simply the different images obtained. The site-dependent I–V curves taken at d_2 overlap each other over most of the investigated voltage range while a tiny splitting among the spectra was observed at the gap voltage higher than 0.3 V. When the topological images are taken at a specific probe–sample distance and voltage, the structure of the topological images can be predicted from the site-dependent I–V curves shown in figure 2.

Only when the site-dependent I–V curves can be clearly distinguished from each other at some selected probe–sample distances and voltages are the site-dependent atomic structures clearly evident in the topographical image. To confirm this statement, the voltage and current parameters used for the topographical images shown in figure 1 are marked by the crosses on the dotted lines in figure 2(a). The less overlapped site-dependent I–V curves at the marked imaging parameters show three topological peaks in the line profile (green/light gray and black) as shown in figure 1(d).

Figure 2(b) shows the site-dependent I–V spectra when a positive gap voltage is applied to the sample. The trend in the current order of magnitude observed at the negative gap voltage is extended to the low positive gap-voltage region. This is expected from the symmetric properties of the electronic structure near the Fermi level. At d_1 the site-dependent I–V curves approach each other as the bias voltage increases and overlap at 0.6 V.

At d_2, when the gap voltage is higher than 0.3 V, the overlapped site-dependent currents start to separate into three distinct curves as shown in figure 2(b). The blue curve, corresponding to the peak in topography, is located below the green curve, which was corresponding to the valley, and the red and green curves, corresponding to the S and V points, become the highest current.

At d_3, the site-dependent current order of magnitude is altered at lower positive gap voltage where the gap distance is shorter. At d_3, the I–V curves for the P and S sites overlap at voltages below 0.1 V and then split in opposite ways at voltages higher than 0.1 V, as shown in figure 2(b). In the I–V curve taken with a negative gap voltage at d_3 shown in figure 2(a), the blue curve, which is corresponding to the P (peak) point in the topographical image of figure 1(c), shows the highest current while the green curve taken at V (valley) shows the lowest current. However, in the I–V curve taken with a positive gap voltage at d_3, shown in figure 2(b), the red I–V curve taken at S (shoulder) in the topographical image shown in figure 1(c) shows the highest current while the blue curve taken at P is the lowest one at voltages above 0.1 V.

This gap-distance-dependent current order of magnitude, for one topological site relative to another, is distinctly different at lower gap voltages when the gap distance is shorter, as just noted. This clearly shows that the switching in the relative current from each site is largely an atomic response variation of the topmost graphene layer on graphite

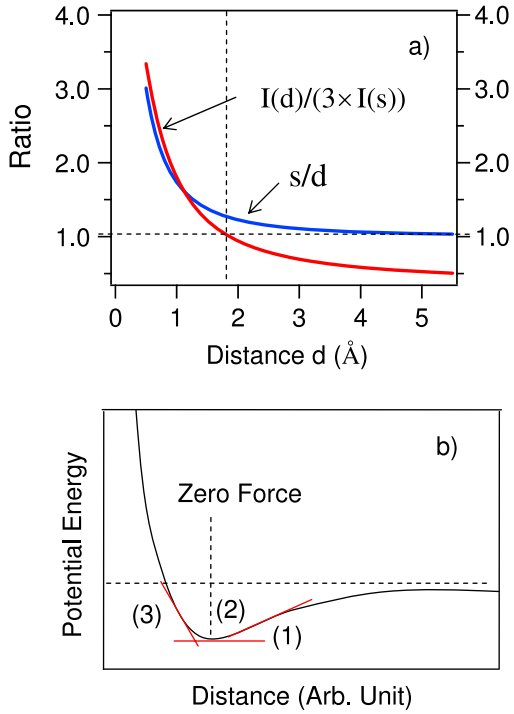

Figure 3. (Colour online) (a) s/d and $I(d)/I(s)$ as a function of the gap distance d and (b) potential curve as a function of the STM probe–sample distance.

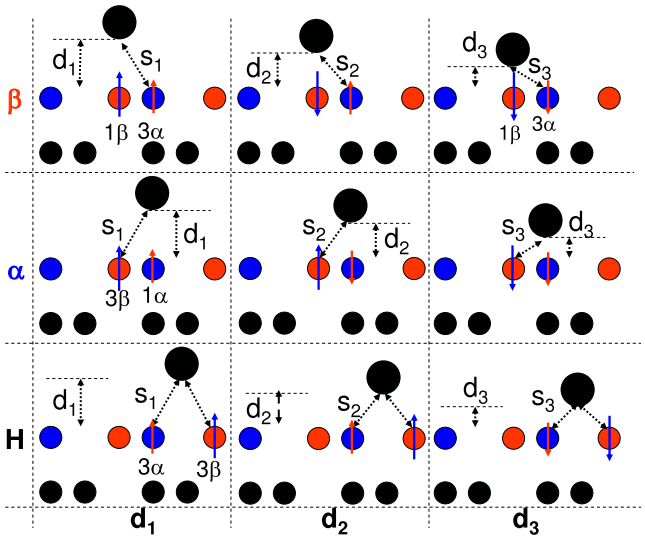

Figure 4. (Colour online) The site-dependent probe–carbon atom interaction is schematically shown when the topmost α-carbon atoms on graphite are indicated by blue and β-carbons by red. Probe atom position varies from β-, α-and H-site along the column but the probe–sample distance varies from d_1, d_2 and d_3 ($d_1 > d_2 > d_3$) in row.

to the external parameters such as the gap distance and the gap voltage rather than the electronic band structure effects, which are independent of the gap distance. Additionally the lower switching voltage at the shorter probe–sample distance strongly suggests that this is not related to the electronic structure alone.

These issues that arise in the gap-distance-dependent imaging and the site-dependent I–V spectra of graphene/graphite are largely related to the STM probe–sample interactions that change as the gap distance varies. The mechanism for the switching of the contrast of the atomic image and the site-dependent I–V spectra from high to low tunneling current (and vice versa) will be discussed below.

4. Site-dependent nearest-neighbor electronic interactions without mechanical response

At a first approximation without any mechanically atomic response, the tunneling current between a probe and the graphite surface is represented by the function of the nearest tip–sample distance and the density of states (DOS) of graphite near the Fermi level (E_F). However, due to the proximity (a_o = 1.42 Å) between α- and β-carbons with distinct electronic and mechanical properties, the contribution of the second-nearest neighbors to tunneling current observed by an STM probe can be significant.

When the site-dependent nearest neighbors are considered on the topmost graphene layer of graphite, each site is surrounded by the electronically and mechanically distinct α- and β-carbons. A β-carbon, an α-carbon and an H–site on the topmost graphene layer are surrounded by three α-carbon atoms, by three β-carbons and by three α- and three β-carbons, respectively.

The tunneling current at each atomic site can be approximated by the sum of the tunneling currents originating from the on-site atom and the nearest off-site carbon atoms, $I_t^{\alpha}(d) = I^{\alpha}(d) + 3I^{\beta}(s)$, $I_t^{\beta}(d) = I^{\beta}(d) + 3I^{\alpha}(s)$ and $I_t^{H}(d) = 3I^{\beta}(s) + 3I^{\alpha}(s)$, where d is the distance between the probe atom and the on-site carbon atom while s is the distance between the probe atom and the nearest off-site atom. The pictorial definition of d and s is shown in figure 4. For an α-site, the tunneling current is mostly determined by three off-site β-atoms rather than the on-site α-atom because the α-atom is electronically inactive for the tunneling but the β-atoms are electronically active at the low gap voltages.

For a β-site, the tunneling current is mostly determined by the on-site β-atom because the three off-site α-carbons are electronically inactive. For an H-site, the tunneling current mostly originated from the three off-site β-atoms because the other three off-site α-carbons are electronically inactive again. Based on this, the α-site and H-site are indistinguishable in the tunneling current because the contribution of three off-site β-carbons to the tunneling current is equivalent where the tunneling current by α-carbon is neglected. This says the only β-site is distinguished from the α- and H-site in tunneling current and predicts the trigonal lattice structures which are typically observed in STM images of HOPG.

To have a better understanding of the predicted trigonal lattice structures, the relative tunneling current magnitude at the β-site is roughly compared with that at the other sites (α- and H-site) as a function of the gap distance, as shown in figure 3(a). The distance ratio (d/s), the distance (d) between the tip atom of a probe and the on-site carbon atom (d) to the distance (s) between the tip atom and the nearest off-site

carbon atom, and the on-site tunneling current to the total off-site tunneling current ratio, $\frac{I(d)}{I(s)} = \frac{I(\text{on-site})_\beta}{3I(\text{off-site})_\beta}$, are roughly estimated as shown in figure 3(a). At the α- and H-sites, the total tunneling current largely originated from three off-site β-carbons. For the estimation, we assume that the potential barrier height is 5 V and the DOS near E_F is constant. The distance ratio is $\frac{s}{d} = \sqrt{1 + \frac{a_0^2}{d^2}}$, where the size of the tip atom and carbon atom is neglected and $a_0 = 1.42$ Å.

As shown in figure 3(a), $I(d)/I(s)$ becomes 1 when s/d is ∼1.3, $I(d)/I(s)$ is ∼1 and d is ∼1.8 Å. At this distance, the tunneling current by three off-site β-carbons is almost equivalent to that by only one on-site β-carbon. This means that the expected tunneling currents at α-, β-and H-sites are almost equivalent to each other and the site-dependent topographical images are almost indistinguishable when the probe tip atom is located where s/d is 1.

However, when s/d is less than 1.3 (large distance), the current ratio is lower than 1. This means that the tunneling current at the β-site is lower than at the α- and H-sites. The β-sites will appear as dark spots instead of a bright spot in the topographical image, while the bright spots with a spheroid bar shape correspond to the combined atomic images of α- and H-sites. As predicted by this argument, the image with a spheroid bar-like structure shown in figure 1(b) can be considered as it is taken at d_2 where $s/d < 1.3$. However, this argument fails to explain the image shown in figure 1(a), which is taken at a larger distance than d_2.

When s/d is higher than 1.3 (short distance), the current ratio is higher than 1. This means that the tunneling current at the β-site is higher than at the α- and H-sites and the bright spots in topographical images are corresponding to β-site carbons. This corresponds to the image shown in figure 1(c).

The analysis implies that the atomic site for the bright spot in the topographical image can be switched from the combined α- and H-sites to the β-site as the gap distance decreases. This could be applicable to explaining the topological images shown figures 1(b) and (c). However, based on the site-dependent nearest-neighbor electronic interaction with the probe tip atom without considering any mechanical response, the analysis for the image at the large gap distance predicts the same pattern of images as the image shown in figure 1(b), rather than the observed image shown in figure 1(a).

5. Atomic image contrast switching

The site-dependent nearest-neighbor electronic interaction only gives a partial explanation for topographical images shown in figure 1. To resolve this, we include the gap-distance-dependent probe–sample mechanical response to the analysis of the images shown in figure 1.

As an STM probe approaches a HOPG sample, the probe feels the van der Waals attractive force between the probe tip atom and a carbon atom on the sample, marked as 1 in figure 3(b). As the probe gets closer to the sample, the attractive force could be a balance with the repulsive force, which is induced by the electronic cloud overlap of the probe tip atom and the atom on the sample, and this is marked as 2 in figure 3(b). As the STM tip further approaches the sample, the repulsive force will dominate over the attractive force, marked as 3 in figure 3(b). The gap-distance-dependent force felt by the probe atom is not limited to the on-site atom on the sample atom but is extended to the nearest off-site atoms on the sample. As explained before, the nearest off-site β-carbon atoms contribute largely to the tunneling current as shown in figure 3(a).

α- and β-carbon atoms respond differently to the force induced by the STM probe because of their distinct mechanical strength. The lateral and vertical mechanical strength can be roughly estimated as below. The overlap integral between the nearest carbons in the plane is about 3 eV while the interlayer overlap integral between the nearest α-carbons and that between the nearest β-carbons is about 0.3 eV and −0.01 eV, respectively [6, 7]. This suggests that the out-of-plane mechanical response of α-carbons to an external mechanical perturbation should be 10 times higher than that of the in-plane response. In particular, the response of β-carbons to the external mechanical perturbation is expected to be 100 times higher than the in-plane response. The possible atomic response to the probe atom is schematically shown in figure 4. The direction of the response is indicated by the arrow direction and the strength is represented by the length of the arrow. The atomic response to the probe should result in the tunneling current.

When s/d is higher than 1.3 (s_3/d_3) as shown in the third column of figure 4, the interaction of the probe atom with the on-site and the nearest off-site carbon atoms is repulsive. As a result, most of the tunneling current is expected from the on-site β-atom and the tunneling current at the β-site should be the highest rather than at the α- and H-sites as expected from figure 3(a). This is applied to give a good explanation for the image shown in figure 1(c).

When s/d is close to 1.3 (s_2/d_2), the probe atom can be located on the on-site carbon atom with repulsive interaction between them while the interaction between the tip atom and the nearest off-site neighbor carbon atoms is attractive, as shown in the second column of figure 4. As a result, the physical response of the nearest site to the probe atom is opposite in direction to that of the nearest off-site. The tunneling current at a β-site is relatively reduced by the repulsive force between the probe and the on-site β-carbon. The attractive forces acting on the off-site β-carbons at α- and H-sites enhance the tunneling currents, which are equivalent to each other. This bidirectional interaction switches the image contrast in the site-dependent tunneling currents and makes the combined image of α- and H-sites brighter while the image of the β-site is darker.

It should be noted that the current ratio is ∼1 where $s/d \sim 1.3$ as shown in figure 3(a). The bidirectional interactions make the current ratio smaller than 1. This is consistent with the line profile shown in figure 1(d). The bidirectional interactions predict that the STM image at the only specific distance ($s/d \sim 1.3$) should be a spheroid bar structure shown in figure 1(b). This specific distance requirement explains why it has not been observed in previous work [8–17].

As the probe is moving away from the sample, the spatial resolution of STM is worse. However, within a relatively

large distance range of d_1 ($s_1/d_1 < 1.3$) while maintaining the atomic resolution, a significant attractive force is acting on the sample. The attractive force by the probe atom acting on the on-site β-atoms is the strongest among the electronically active β-atoms because the van der Waals interaction is rapidly weaker with distance, as shown in figure 3(b). The on-site β-carbon will respond strongly to the attractive force towards the probe compared to the off-site β-carbons. Due to this differential mechanical response, the brighter spots in the image shown in figure 1(a) correspond to β-atoms as long as the probe is located not far from the sample, even though the current ratio without considering the mechanical response shown in figure 3(a) indicates that the current at the α- and H-sites is higher than that at the β-site. Now the observation shown in figure 1(a) is successfully explained by considering the mechanical response.

All of the topographical images shown in figure 1 are fully explained. The analysis shows that the atomic image contrast is switched as the probe–sample distance varies. There is a critical distance to observe the combined image of an α- and a H-site and this appears as a spheroid bar structure, which has not been observed before.

6. Changes in the relative current at different topological sites

To understand the voltage-dependent current magnitude for different topographical sites relative to one another, as shown in figure 2, the attractive electrostatic interaction between the probe and the topmost graphene layer on graphite is taken into account.

At d_1 (large distance), the van der Waals interaction is effectively acting on on-site carbon atoms as explained before. However, the electrostatic interaction is a long range attractive force compared to the van der Waals interaction. As the result, the electrostatic interaction acts on not only the on-site carbon atoms but also the off-site carbon atoms. As the voltage increases, the contribution of the off-site β-carbons to the tunneling current is larger due to the larger electrostatic attractive interaction with the off-site β-carbons. As the result, the difference in the current at the β-site and at the other sites (α- and H-sites) becomes smaller as the bias voltage increases, as shown in figure 2.

When $s/d \sim 1.3$ (intermediate distance) and $I(d)/I(s) \sim 1$, figure 3(a) indicates that there is no significant difference among the tunneling currents at β-, α-and H-sites when the mechanical response is ignored. However, this prediction disagrees with the experimentally observed difference I–V curves shown in the inset of figure 2(a). The difference spectra clearly show the tunneling current spectra at P and S observed at d_2 and it shows they are almost overlapping but they are distinct from the tunneling current spectra at V. The difference spectra are consistent with the line profile shown in figure 1(d) and the topographical image shown in figure 1(b).

As the gap voltage increases, the on-site repulsive force can be reduced by the electrostatic attraction but it is weak compared to the high strength of the repulsive force. However, the total force acting by the probe tip atom on the off-site β-carbons is the sum of the attractive van der Waals force and the electrostatic attractive force, as shown in the second column of figure 4. As the gap voltage increases over 0.2 V, the electrostatic interaction increases the strength of the total attractive force to the nearest off-site atoms. This indicates that the relative tunneling current magnitude from the three nearest off-site β-carbons is getting higher with increasing gap voltage compared to the current from the on-site β-carbon. This causes the switching of the current order of magnitude and separation of the overlapped I–V curves above 0.3 V as shown in figure 2. The lowest current among the separated I–V curves above 0.3 V of the bias voltage corresponds to the current at the β-site while the currents at the α- or H-sites are still almost equivalent.

At d_3 (short distance), the clear current order of magnitude of one topological site relative to another (as discussed above) changes at the positive gap voltage, 0.1 V (figure 2(b)), while the site-dependent curves overlap at voltages higher than 0.3 V in magnitude in the negative gap-voltage region (figure 2(a)). The site-dependent I–V curve difference is higher with positive gap bias voltage and the site-dependent current voltage curves are clearly distinguishable at voltages higher than 0.2 V, as shown in figure 2(b). This implies that the equivalent property between α- and H-sites is not maintained anymore as the bias voltage increases. The bias polarity-dependent behavior is related to the field enhancement and resonant interaction discussed in the following.

The current magnitude of one topological site relative to another (as discussed above) is not the result of the voltage-dependent electronic structure of graphene and graphite, which have symmetric occupied and unoccupied electronic structures within 1 eV [6–8, 13, 18]. The site-dependent tunneling current order of magnitude is altered at gap voltages much lower than 0.8 V and it strongly depends on the polarity of the bias voltage: if the electronic structure played a role, a different outcome would be expected for this system. While charge density waves are seen at low bias voltages and in fact are dependent on the polarity of the bias voltage, the effects reported here are also not the results of charge density waves: what is seen here is related to structure, not the Fermi level crossings.

Typically the electrostatic force is proportional to the square of the gap voltage [19]. By incorporating the electrostatic influence in the tunneling current, the tunneling spectra shown in figure 2 are fitted with $I(V) = aV\mathrm{e}^{bV^2}$ and the fitting coefficients of a and b are plotted for peak (P), shoulder (S) and valley (V) sites, respectively, in figure 5. The coefficient a (conductance at low voltage) largely represents the exponentially dependent tunneling current as a function of the probe–sample distance at low gap-voltage, while the coefficient b in the exponent depends on the inverse of the probe–sample distance at high gap voltage. The details are shown in the figure caption of figure 5. The coefficient a corresponding to the conductance at low gap voltage almost linearly increases with the inverse of the gap distance, as expected.

The coefficient a for the positive gap voltage is less than that for the negative gap voltage. This means that the

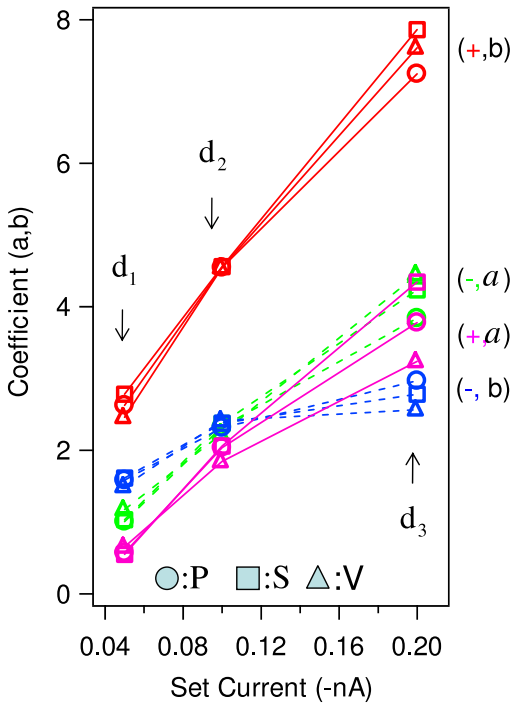

Figure 5. (Colour online) The site-dependent fitting coefficients when the tunneling current spectra of figure 2 are fitted by a function, $I(V) = aV\mathrm{e}^{bV^2}$, are obtained by incorporating the contribution of the electrostatic force of $F_{\mathrm{es}} \propto V^2$ where $a \propto \mathrm{e}^{-1.025\sqrt{\Phi}d}$, $b \propto \frac{1}{d}\sqrt{\Phi}$, Φ is the potential barrier height and d is the STM probe-to-sample distance.

conductance at negative gap voltage is higher than that at positive gap voltage. This suggests that electrons could be emitted from a relatively large area of the sample.

At the gap distance of d_3, the coefficient a at positive gap voltage largely depends on the site. These site-dependent coefficients mean that the conductance at low bias voltage depends on the site. This strongly suggests that the electronic property at the on-site, such as the density of states near the Fermi level, largely depends on the type of atoms. This site-dependent conductance originated from the distinguished site-dependent electronic properties.

The coefficient b for positive gap voltage is almost twice that for the negative gap voltage, as shown in figure 5. Their difference is higher with smaller gap distance. This strongly suggests that the interaction between the probe atom and the surface carbon atoms largely increases with a positive gap voltage. This bias polarity-dependent interaction and the coefficient difference are attributed to not only the emission efficiency of electrons by the field-enhanced probe tip [20] but also the resonant force between the probe atom and the surface carbon atom [21].

The enhanced tunneling conductivity at lower gap distance and higher positive gap voltage increases the resonance force, which is proportional to the conductance due to the resonance interactions between the sample and the probe atom [21]. The enforced attractive interaction by higher current and positive gap voltage breaks the symmetrical tunneling behavior at α- and H-sites. An α-site is surrounded by three β-carbons but an H-site is surrounded by three β-carbons as well as three α-carbons. The primary resonant interaction of the probe atom with the surface carbons will occur with the off-site β-carbons. However, as the tunneling current increases, the on-site α-site carbon atom will be participating at the resonant interaction. This makes the separation of the overlapped site-dependent I–V spectra visible as well as altering the order of the site-dependent currents at lower gap voltages, as illustrated in figure 2(b).

The distinguishable site-dependent tunneling I–V curve separation suggests that a genuine hexagon-like structure can be obtained at a short gap distance with a positive high gap voltage to the sample. The previously rarely reported hexagonal structures might be obtained by using the imaging parameters suggested by this study such as a low gap distance and a high positive voltage [11] while there is no significant deformation on the layer structure.

7. Electronic structure versus lattice distortion

The electronic structure of graphite strongly suggests that one out of two carbon atoms is imaged by STM at low gap voltages. This indicates that the imaged carbon atoms correspond to β-carbons. However, without introducing the proposed distortion, the experimentally obtained images and the current order of magnitude switching were not fully understood, as described above. The in-plane interaction is stronger by a couple of orders of magnitude than the inter-plane interaction, as indicated by the overlap integral strength explained above. The overlap integral between inter-plane β-carbons is much weaker than that between inter-plane α-carbons. As a result, the significant mechanical response to the probe tip atom is expected from β-carbons. By incorporating this differential atomic response to the probe tip atom, the observed atomic images and the current order of magnitude are fully explained.

8. Conclusions

This study shows that the atomic image of the topmost graphene layer on graphite is varied with the tunneling gap distance. The atomic image variation corresponds to the switching of the atomic image contrast. This is attributed to the probe–sample distance-dependent atomic response of α- and β-carbons with the distinct electronic and mechanical properties, and the distinct site-dependent nearest off-site neighbors of the topmost graphene layer on graphite. Additionally the switching of site-dependent tunneling current order of magnitude is observed and understood as the differential electrostatic and resonant atomic response of the topmost graphene layer on graphite to the STM probe.

Acknowledgment

This work was supported by the Korea Research Foundation Grant funded by the Korean Government (KRF-2008-313-C00316).

References

[1] Novosselov K S, Geim A K, Morozov S V, Jiang D, Katsnelson M I, Grigorieva I V, Dubonos S V and Firsov A A 2005 *Nature* **438** 197

[2] Geim A K and Novoselov K S 2007 *Nat. Mater.* **6** 183

[3] Meyyappan M 2005 *Carbon Nanotubes-Science and Applications* (Boca Raton, FL: CRC Press)

[4] Dresselhaus M S, Dresselhaus G and Eklund P C 1996 *Science of Fullerenes and Carbon Nanotubes: Their Properties and Applications* (Amsterdam: Elsevier)

[5] Hembacher S, Giessibl F J, Mannhart J and Quate C F 2003 *Proc. Natl Acad. Sci. USA* **100** 12539

[6] Partoens B and Peeters F M 2006 *Phys. Rev.* B **74** 075404

[7] Wallace P R 1947 *Phys. Rev.* **71** 622

[8] Tomanek D, Louie S G, Jonathon M H, Abraham D W, Thomson R E, Ganz E and Clarke J 1987 *Phys. Rev.* B **35** 7790

[9] Binnig G, Fuchs H, Gerber Ch, Rohber H, Stoll E and Tosatti E 1986 *Europhys. Lett.* **1** 31

[10] Pardes J I, Martinez-Alonso A and Tascon J M D 2001 *Carbon* **39** 473

[11] Wang Y, Ye Y and Wu K 2006 *Surf. Sci.* **600** 729

[12] Ouseph P J, Poothackanal T and Mathew G 1995 *Phys. Lett.* A **205** 65

[13] Gwo S and Shih C K 1993 *Phys. Rev.* B **47** 13059

[14] Kilic C, Mehrez H and Ciraci S 1998 *Phys. Rev.* B **58** 7872

[15] McKinnon B A and Choy T C 1996 *Phys. Rev.* B **54** 11777

[16] Atamny F, Spillecke O and Schlogl R 1999 *Phys. Chem. Chem. Phys.* **1** 4113

[17] Soler J M, Bao A M, Garcia N and Rohrer H 1986 *Phys. Rev. Lett.* **57** 444

[18] Sacks W, Roditchev D and Klein J 1998 *Phys. Rev.* B **57** 13118

[19] Hao H W, Baro A M and Saenz J J 1991 *J. Vac. Sci. Technol.* B **9** 1323

[20] Lucas A A, Cutler P H, Feuchtwang T E, Tsong T T, Sullivan T E, Yuk Y, Nguyen H and Silverman P J 1988 *J. Vac. Sci. Technol.* A **6** 461

[21] Chen C J 1991 *J. Phys.: Condens. Matter* **3** 1227